

Nonlinear study of tearing modes and plasma flows around magnetic islands in tokamak plasmas

Cite as: AIP Advances **10**, 075005 (2020); <https://doi.org/10.1063/5.0013209>

Submitted: 08 May 2020 . Accepted: 07 June 2020 . Published Online: 01 July 2020

Jizong Yang, Jingchun Li , Jiaqi Dong, Songfen Liu, Peng Shi, Yizhen Zhao, and Shaoyong Chen

COLLECTIONS

Paper published as part of the special topic on [Chemical Physics](#), [Energy, Fluids and Plasmas](#), [Materials Science](#) and [Mathematical Physics](#)



View Online




Export Citation




CrossMark





Sign up for topic alerts
New articles delivered to your inbox



Nonlinear study of tearing modes and plasma flows around magnetic islands in tokamak plasmas

Cite as: AIP Advances 10, 075005 (2020); doi: 10.1063/5.0013209

Submitted: 8 May 2020 • Accepted: 7 June 2020 •

Published Online: 1 July 2020



Jizong Yang,¹ Jingchun Li,^{1,2,a)}  Jiaqi Dong,³ Songfen Liu,¹ Peng Shi,³ Yizhen Zhao,¹ and Shaoyong Chen⁴

AFFILIATIONS

¹Nankai University, Tianjin 421001, People's Republic of China

²University of California, Irvine, California 92697, USA

³Southwestern Institute of Physics, P.O. Box 432, Chengdu 610041, People's Republic of China

⁴College of Physics, Sichuan University, Chengdu 610065, People's Republic of China

^{a)} Author to whom correspondence should be addressed: jingchunli@pku.edu.cn

ABSTRACT

The behavior of non-linear tearing modes and the plasma flows around magnetic islands is studied numerically in a cylindrical geometry using the method of reduced magneto-hydro-dynamic simulation. The results show that the single tearing mode (STM) becomes stable in a short time. The magnetic islands of double tearing modes (DTMs) first develop to a sufficiently large scale and then couple together when entering the non-linear phase. It is also shown that, before the non-linear growth stage, the perturbed kinetic energy and magnetic energy of both the STM and DTM have a process from different signs to constant positive values. For the STM island and plasma flow, it is demonstrated that the shear flow is formed on both sides of the islands and the poloidal flow velocity around the O-point is larger than that around the X-point. For the DTM island and plasma flow, we found that the peak of the poloidal flow velocity is mainly distributed at the O-point edge and the X-point of the magnetic island and the plasma flow velocities at the magnetic island edges are opposite. In addition, the process of plasma flow accompanying the nonlinear evolution of tearing modes is also presented.

© 2020 Author(s). All article content, except where otherwise noted, is licensed under a Creative Commons Attribution (CC BY) license (<http://creativecommons.org/licenses/by/4.0/>). <https://doi.org/10.1063/5.0013209>

I. INTRODUCTION

Advanced tokamak operations have been studied adequately because of their higher bootstrap current fraction and the significant transport improvement obtained with reversed magnetic shear. The double tearing mode (DTM) instability induced by the negative magnetic shear, s , is an important magneto-hydro-dynamic (MHD) instability, which leads to energy loss through magnetic reconnection and even causes plasma disruption.^{1–7} On the other hand, MHD flow layers, which have an important effect on plasma confinement, are demonstrated to merge in the development of the DTM.⁴ The density profile peaking inside the magnetic island is observed in some experiments, which suggests that the plasma electric potential may have some structures inside the magnetic islands.⁸ Therefore,

the interaction between the flow structure and the magnetic island becomes an important issue in improving plasma confinement and transport.^{9,10}

The experiments and correlation analyses about the temporal-spatial behaviors of plasma flows and turbulence show that the flow has similar structures as the magnetic island. Observations on a large helical device show that the flattening of the ion temperature and electric potential is observed inside the magnetic island when the $n/m = 1/1$ perturbation field is applied. The sheared poloidal flows and sheared radial electric field are also observed at the boundaries of the magnetic island because of the missing poloidal flow inside the static magnetic island.⁸ Furthermore, Zhao *et al.* found that the sign of the potential fluctuation for the flows inverses and the power significantly reduces at the $q = 3$ surface. The flow structure depends

on the locations of the magnetic island. Usually, the flows are concentrated on the boundary of the magnetic island with an elongated structure, while the turbulence is concentrated near the X-point of the magnetic island.¹⁰

Theoretically, the research on the tearing mode and the flows near the magnetic islands during their formation has been an important topic in recent years.^{11,12} In the study of tearing modes, in terms of the linear and nonlinear behavior of the DTM under the cylindrical geometry, it is found that the distance between the two rational planes has a great influence on the evolution of the magnetic island.¹² In addition, early studies have shown that the shear flow, which is usually strong enough to suppress the turbulent flow,¹³ will appear at the edge of the magnetic island in the quasi-linear stage of the evolution of the tearing mode. The authors of Refs. 14–16 studied a MHD flow driven by the energy of the magnetic field released during the evolution of the tearing mode. They mainly analyzed the characteristics of the tearing mode under the influence of anomalous electron viscosity and plasma resistance in the slab geometry¹⁷ and gave the scaling relationship of the linear growth rate of the tearing mode. Both in the linear and nonlinear phase, the stabilizing effect of shear flow on the tearing mode has been verified by numerical simulation.^{18,19} The authors of Ref. 20 applied a simplified magnetic fluid model to study the evolution process and steady-state characteristics of zonal magnetic islands under the influence of local flow. In sum, there exists a study of nonlinear tearing modes and the plasma flows around the islands based on the reduced MHD model. However, the preliminary results are in slab geometry, and a predictive investigation of tearing mode interactions with plasma flow around magnetic islands under a cylindrical geometry is essential for future fusion experiments.

In this work, we numerically investigate the nonlinear behavior of single tearing modes (STMs), the DTM, and the plasma flows around the magnetic islands based on the reduced MHD model in a cylindrical geometry. The temporal-spatial behaviors of the nonlinear tearing modes are analyzed, focusing on the magnetic island structure, plasma flows, perturbed kinetic energy, and perturbation of magnetic energy. The growth rates of the STM and DTM have a similar evolution process before entering the nonlinear phase. After that, the STM reaches a static state, while the DTM still holds on to a complicated evolution process. Furthermore, it is demonstrated that the plasma flows, which are mainly concentrated on the boundary of the magnetic island with an elongated structure, have similar structures as the magnetic island. The spatial structures concentrated near the X-point and trapped inside the magnetic island are also observed.

The rest of this paper is organized as follows. The physics model is introduced in Sec. II. In Sec. III, we report the results of the numerical study for single and double tearing modes and the plasma flow around the corresponding magnetic islands. Brief conclusions are given in Sec. IV.

II. MODELING

We start from the generalized Ohm's law and the equation of motion,

$$\mathbf{E} + \frac{1}{c} \mathbf{V} \times \mathbf{B} = \eta \mathbf{j} - \eta_2 \nabla_\perp^2 \mathbf{j}, \quad (1)$$

$$\rho \left[\frac{\partial \mathbf{V}}{\partial t} + (\mathbf{V} \cdot \nabla) \mathbf{V} \right] = -\nabla p + \frac{1}{c} \mathbf{j} \times \mathbf{B} + \mu \nabla^2 \mathbf{V}. \quad (2)$$

For a tokamak with a large aspect-ratio, the magnetic field configuration can be approximated by a cylinder coordinate system (r, z, θ) . Assuming an incompressible plasma, $\nabla \cdot \mathbf{V} = 0$ and $\nabla \cdot \mathbf{B} = 0$, then, the magnetic field and plasma velocity can be expressed by the following two scalar potentials: the magnetic flux function Ψ and the fluid velocity potential function Φ . In addition, we have

$$\mathbf{B} = B_0 \hat{z} + \nabla \Psi \times \hat{z}, \quad (3)$$

$$\mathbf{V} = V_0 \hat{z} + \nabla \Phi \times \hat{z}. \quad (4)$$

The electromagnetic field equations in the Gaussian unit system are

$$\nabla \times \mathbf{B} = \frac{4\pi}{c} \mathbf{j}, \quad (5)$$

$$\nabla \times \mathbf{E} = -\frac{1}{c} \frac{\partial \mathbf{B}}{\partial t}. \quad (6)$$

From Eq. (5), we can get

$$\mathbf{j} = \frac{c}{4\pi} \nabla \times (\nabla \Psi \times \hat{z}) = \frac{c}{4\pi} \left(\frac{\partial}{\partial z} \nabla \Psi - \hat{z} \nabla_\perp^2 \Psi \right). \quad (7)$$

Substituting Eq. (6) into Eq. (1), we can get

$$\frac{\partial \Psi}{\partial t} = -B_0 \frac{\partial \Phi}{\partial z} - [\Psi, \Phi] + \frac{c^2}{4\pi} [\eta \nabla_\perp^2 \Psi - \eta_2 \nabla_\perp^2 (\nabla_\perp^2 \Psi)] + c E_{wz}. \quad (8)$$

Here, Poisson's bracket is defined as

$$[a, b] = \frac{1}{r} \left(\frac{\partial a}{\partial r} \frac{\partial b}{\partial \theta} - \frac{\partial b}{\partial r} \frac{\partial a}{\partial \theta} \right) = (\nabla a \times \nabla b) \cdot \hat{z},$$

$$\hat{z} \cdot \nabla \times \frac{d\mathbf{v}}{dt} = \frac{1}{\rho} \hat{z} \cdot \nabla \times \left(-\nabla P + \frac{1}{c} \mathbf{j} \times \mathbf{B} + \mu \nabla^2 \mathbf{v} \right). \quad (9)$$

The left side of Eq. (9) is as follows:

$$\begin{aligned} \hat{z} \cdot \nabla \times \frac{d\mathbf{V}}{dt} &= -\frac{d}{dt} \nabla_\perp^2 \Phi \\ &= -\left[\frac{\partial}{\partial t} \nabla_\perp^2 \Phi + (\mathbf{V} \cdot \nabla) \nabla_\perp^2 \Phi \right] \\ &= -\left[\frac{\partial}{\partial t} \nabla_\perp^2 \Phi + \nabla \Phi \times \hat{z} \cdot \nabla (\nabla_\perp^2 \Phi) \right]. \end{aligned} \quad (10)$$

The first term on the right side of Eq. (9) is given as follows:

$$\nabla \times \nabla P = 0. \quad (11)$$

The second term on the right side of Eq. (9) is given as follows:

$$\frac{1}{\rho c} \hat{z} \cdot \nabla \times (\mathbf{j} \times \mathbf{B}) = -\frac{B_0}{4\pi \rho} \frac{\partial}{\partial z} \nabla_\perp^2 \Psi - \frac{1}{4\pi \rho} [\nabla_\perp^2 \Psi, \Psi]. \quad (12)$$

The third term on the right side of Eq. (9) is given as follows:

$$\frac{\mu}{\rho} \hat{z} \cdot \nabla \times \nabla_\perp^2 \mathbf{V} = -\frac{\mu}{\rho} \nabla_\perp^2 (\nabla_\perp^2 \Phi). \quad (13)$$

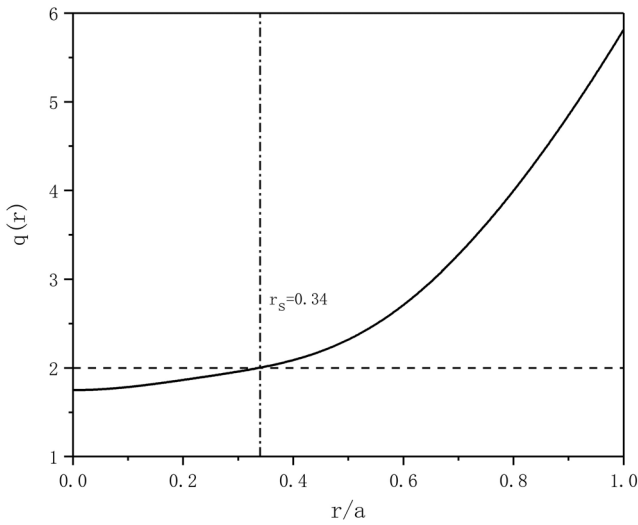


FIG. 1. The safety factor profile used for a single tearing mode calculation.

Substituting Eqs. (10)–(13) into Eq. (9), then, we get

$$\begin{aligned} \frac{\partial}{\partial t} \nabla_{\perp}^2 \Phi = & -\frac{B_0}{4\pi\rho c} \frac{\partial}{\partial z} \nabla_{\perp}^2 \Psi - [\nabla_{\perp}^2 \Phi, \Phi] \\ & + \frac{1}{4\pi\rho} [\nabla_{\perp}^2 \Psi, \Psi] + \frac{\mu}{\rho} \nabla_{\perp}^2 (\nabla_{\perp}^2 \Phi). \end{aligned} \quad (14)$$

Equations (8) and (14) can be normalized into

$$\frac{\partial \psi}{\partial t} = \frac{\partial \phi}{\partial \zeta} - [\psi, \phi] + S^{-1} \widehat{\nabla}_{\perp}^2 \psi - R^{-1} \widehat{\nabla}_{\perp}^2 (\widehat{\nabla}_{\perp}^2 \psi) + E_{wz}, \quad (15)$$

$$\frac{\partial}{\partial t} \widehat{\nabla}_{\perp}^2 \phi = -\frac{\partial}{\partial \zeta} \widehat{\nabla}_{\perp}^2 \psi - [\widehat{\nabla}_{\perp}^2 \phi, \phi] + [\widehat{\nabla}_{\perp}^2 \psi, \psi] + R_{\mu}^{-1} \widehat{\nabla}_{\perp}^2 (\widehat{\nabla}_{\perp}^2 \phi), \quad (16)$$

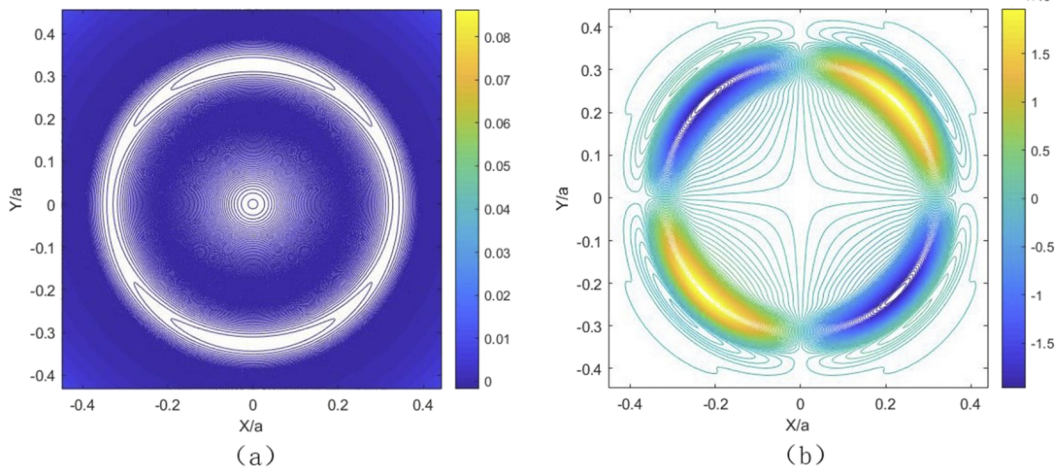


FIG. 2. Contours of magnetic flux (a) and electrostatic potential (b) of the single tearing mode at $t = 420$, $R = 10^8$, and $S = 10^{18}$.

where t is normalized to $\tau_h t$, r is normalized to ar , $\zeta \equiv z/R_0 q(a)$, $\psi = \Psi/aB_0$, $\phi = \Phi/(a^2/\tau_h)$, and the magnetic Reynolds number $S \equiv \tau_\eta/\tau_h$, with $\tau_\eta = 4\pi a^2/\eta c^2$ being the magnetic diffusion time. The electron viscosity magnetic Reynolds number is $R \equiv \tau_v/\tau_h$, with $\tau_v = 4\pi a^4 n_e^2 e^2/m_e \mu_e c^2$ being the electron viscosity induced current diffusion time, and $R_\mu = \tau_\mu/\tau_h$, with $\tau_\mu = \rho a^2/\mu$ being the plasma momentum diffusion time.

The form of the q distribution function used is as follows:

$$q(r) = q_c \left\{ 1 + \left(\frac{r}{r_0} \right)^{2\lambda} \right\} \left[1 + A \exp \left\{ - \left(\frac{r - r_\delta}{\delta} \right)^2 \right\} \right]. \quad (17)$$

In the numerical simulation of the single tearing mode, the parameters are fixed as follows: $\lambda = 1$, $r_0 = 0.37$, $\delta = 0.34$, $r_\delta = 0$, $A = 1.5$, $q_c = 0.7$, and the position of the $q = 2$ surface $r_s = 0.34$. For the simulation of the double tearing mode, the parameters are fixed as follows: $\lambda = 1$, $r_0 = 0.412$, $\delta = 0.273$, $r_\delta = 0$, $A = 3$, $q_c = 1.05$, the positions of $q = 3$ surfaces $r_{s1} = 0.31$ and $r_{s2} = 0.53$, and the distance between the surfaces $D_{12} = 0.22$. The nonlinear behavior of the STM, DTM, and plasma flows around the islands is simulated. The character of the nonlinear evolution of both the STM and DTM is estimated by perturbed total kinetic energy $E^{kin} = |\nabla \tilde{\phi}|^2$.⁵

III. NUMERICAL RESULTS

In this part, we will report our simulation results of non-linear behaviors of tearing modes, the plasma flows around the magnetic islands, and the interactions between them.

A. Single tearing modes and plasmas flows around magnetic islands

For the q distribution function Eq. (12), we gave the parameters for the STM, as mentioned before. The corresponding monotonic q distribution is shown in Fig. 1. The position of the rational surface r_s is located at 0.34.

Figure 2 shows the contours of magnetic flux (a) and electrostatic potential (b) of the single tearing mode at $t = 420$.

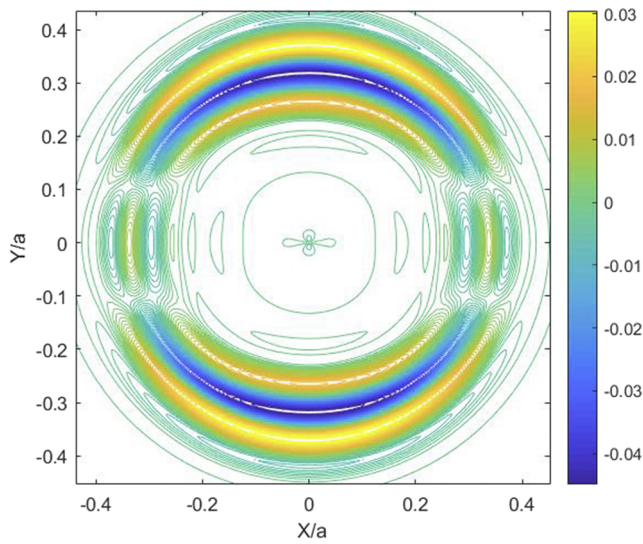


FIG. 3. Contour of the poloidal velocity distribution of single tearing modes at $t = 420$, $R = 10^8$, and $S = 10^{18}$.

It shows that the evolution process of the single tearing mode is relatively simple. In the stage of steady growth of the single tearing mode, two magnetic islands grow at the rational surface and form a flow field distribution.

Figure 3 shows the contour of poloidal velocity flow of single tearing modes at $t = 420$. From Fig. 3, we can see that in the process of generating the magnetic island, the acceleration of the plasma by the bending of the magnetic lines of force leads to a certain degree of poloidal flow velocity distribution. Shear flow is formed on both sides of the magnetic island, and the poloidal flow velocity is larger around the O-point than around the X-point of the magnetic island. There is also a small peak in the poloidal flow velocity at the X-point, while the amplitude of the poloidal flow velocity is weaker at other locations.

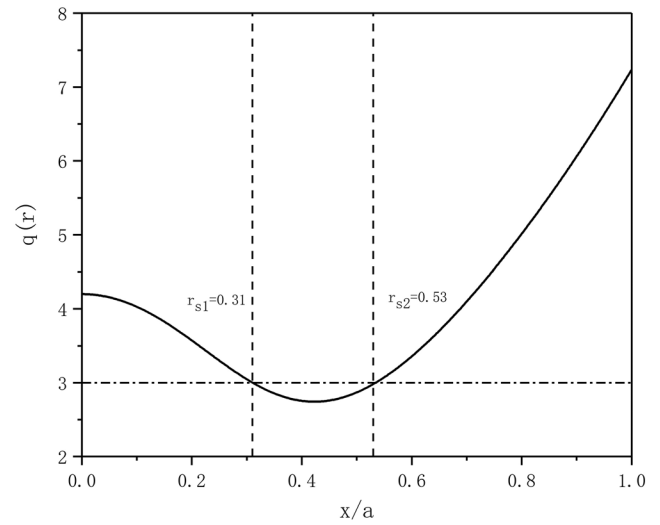


FIG. 5. The safety factor profile used for double tearing mode calculations, for which the parameters are fixed as $\lambda = 1$, $r_0 = 0.412$, $\delta = 0.273$, $r_\delta = 0$, $A = 3$, $q_c = 1.05$, the positions of $q_s = 3$ resonant flux surfaces $r_1 = 0.3107$ and $r_2 = 0.5345$, and the distance between the two resonant flux surfaces $D_{12} = 0.22$.

Figure 4 shows the evolution of the growth rate (a) and perturbed kinetic energy (b) of single tearing modes. From Fig. 4(a), we can see that from about $t = 100$, the growth rate becomes a positive value and gradually increases. When it reaches about $t = 140$, it tends to be stable and the stable growth rate γ is 0.012. Figure 4(b) shows that the initial perturbed magnetic energy decreases rapidly and then enters a rapid rise phase. At the same time, the perturbed kinetic energy line increases rapidly and then decreases and the changes in them are opposite. After a period of oscillating, they came into a steady stage after $t = 140$ when the growth rate is close to zero.

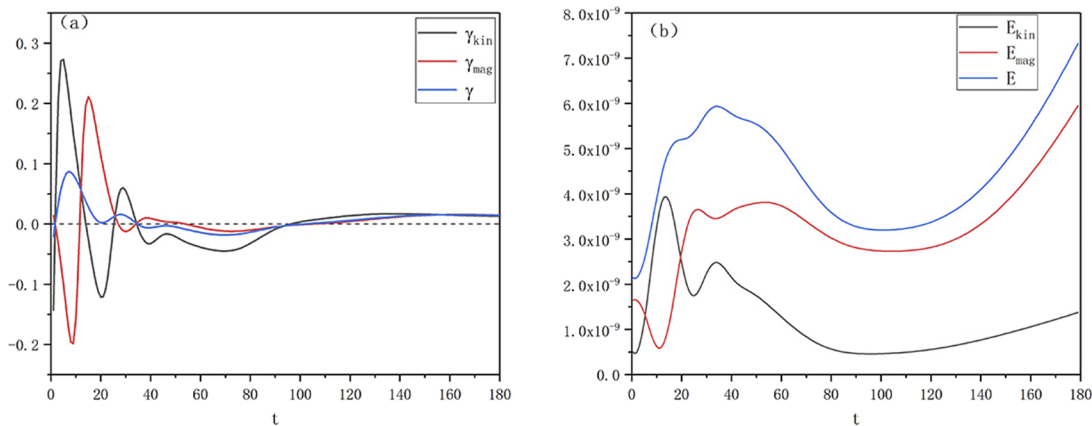


FIG. 4. The evolution of the growth rate (a) and perturbed kinetic energy (b) of single tearing modes.

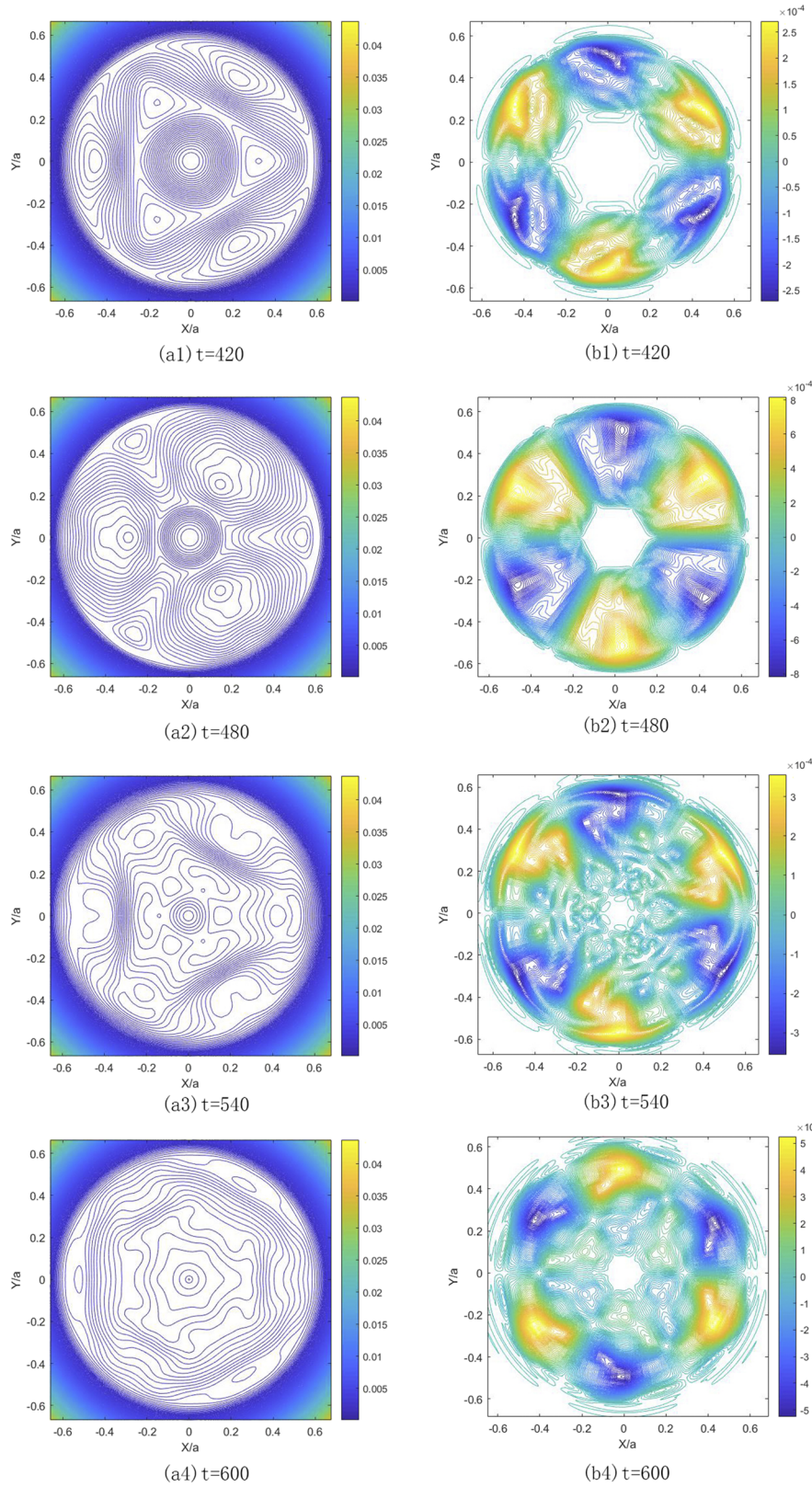


FIG. 6. Contours of magnetic flux (a) and electrostatic potential (b) at different times with [(a1) and (b1)] $t = 420$, [(a2) and (b2)] $t = 480$, [(a3) and (b3)] $t = 540$, [(a4) and (b4)] $t = 600$, and $D_{12} = 0.22$, $R = 10^8$, and $S = 10^{18}$.

B. Double tearing modes and plasmas flows around magnetic islands

For the DTM, the distance between the two rational surfaces depends on q_c , which is set to be 1.05 here so that the two $q = 3$ and 1 rational surfaces are located at $r_{s1} = 0.3107$ and $r_{s2} = 0.5345$, respectively, and the distance between them is 0.2238. The safety factor profile is shown in Fig. 5.

Figure 6 shows the contours of magnetic flux (a) and electrostatic potential (b) at different times. It gives the evolution of magnetic islands and magnetic field lines against time. We could see that in the initial period, at $t = 250$, the magnetic islands appeared on the two rational surfaces and the positions were staggered. Divided by the central equilibrium magnetic field lines, the two magnetic islands evolve on their own rational surfaces. When the scale of the magnetic island grows to a certain degree ($t = 420$), it can be seen that the radial positions of the two groups of magnetic islands coincide; from $t = 440$ to 480, when the inner magnetic island connects the equilibrium magnetic field lines in the middle, the width of the inner magnetic island begins to decrease, the magnetic island deforms, and then it moves outward. At the same time, the width of the outer magnetic island continues to increase and moves inward.

At $t = 500$, the migration process of the inside and outside magnetic islands is basically completed. Afterward, the outer magnetic islands begin to reconnect with the outer equilibrium magnetic field lines and the inner magnetic islands begin to reconnect with the inner equilibrium magnetic field lines. The outer magnetic reconnection process is tremendously faster than that of the inner side. As the magnetic reconnection process progressed, the magnetic islands gradually disappeared and new magnetic field lines were generated. As can be seen from $t = 520$ and 540, during the disappearance of the first batch of magnetic islands, a new batch of magnetic islands is produced. However, the scales of the new ones are significantly smaller than those of the first batch. Some of them disappear after a period of evolution at the generating position, and some of them disappear after moving to a certain position in the radial direction. Generally, their behavior is similar to the first batch of

magnetic islands. After that, the process of magnetic island generation and disappearance was repeated for many times, but the scale was much smaller than that of the first two, and eventually, the magnetic islands disappeared.

The evolution process of the magnetic field lines corresponds to Fig. 6. Here, we analyze this process from the perspective of perturbed magnetic energy and kinetic energy. Figure 7 represents the evolution of perturbed magnetic energy (a) and kinetic energy (b) of the DTM with different modes. From Fig. 7, it can be seen that the two modes, namely, $m/n = 0/0$ and $3/1$, play a major role. During the time from $t = 0$ to $t = 250$, there is no obvious change in magnetic energy in this initial stage. During the period from $t = 250$ to $t = 400$, the width of the magnetic island is in the slowly increasing growth period and the corresponding perturbed magnetic energy also begins to increase slowly. From $t = 400$ to $t = 500$, the magnetic islands in the inner and outer layers exchange positions and the perturbed magnetic energy increases rapidly. After $t = 500$, the initial magnetic islands disappear and some weaker magnetic islands repeatedly disappear, and basically, they stabilize after $t = 700$, as can be seen from the fluctuation phase of the perturbed magnetic energy shown in Fig. 7. We do some quantitative analysis of the results in Fig. 7. It can be seen that the stage is the linear stage of the DTM before $t = 200$ and the DTM enters a nonlinear period around $t = 300$. The perturbed magnetic energy is dominated by $m/n = 3/1$ and $0/0$, both of which are of the same magnitude and more than three orders of magnitude higher than the other modes. In the linear stage, the growth rate of perturbed magnetic energy is 0.03 and 0.01 for $m/n = 3/1$ and $0/0$ modes, respectively. Subsequently, in the process of entering the nonlinear phase, the growth rate of the $m/n = 3/1$ mode decreases, while that of the $m/n = 0/0$ mode increases rapidly and becomes significantly higher than that of the other modes. At the same time, the perturbed magnetic energy of the high m mode has also developed rapidly. The modes of $m/n = 0/0$, $3/1$, $6/2$, and $9/3$ are all taken into account in the analysis. Their ratio of their peaks is about 55:5.5:5:1. The value is approximately equal to 43:8:1 when reaching equilibrium. It should be noted that the value of $m/n = 0/0$ is too large here, so only the last three are considered.

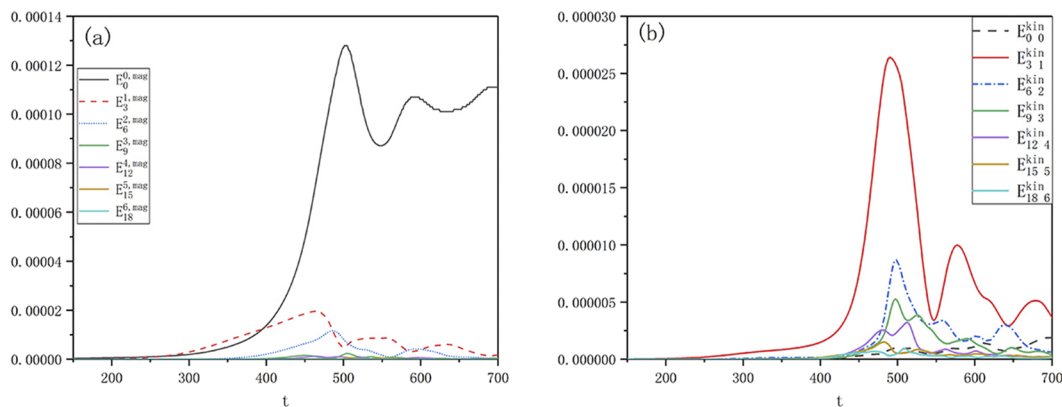


FIG. 7. Evolution of perturbation magnetic energy (a) and kinetic energy (b) corresponding to the double tearing mode with different modes with $R = 10^8$ and $S = 10^{18}$.

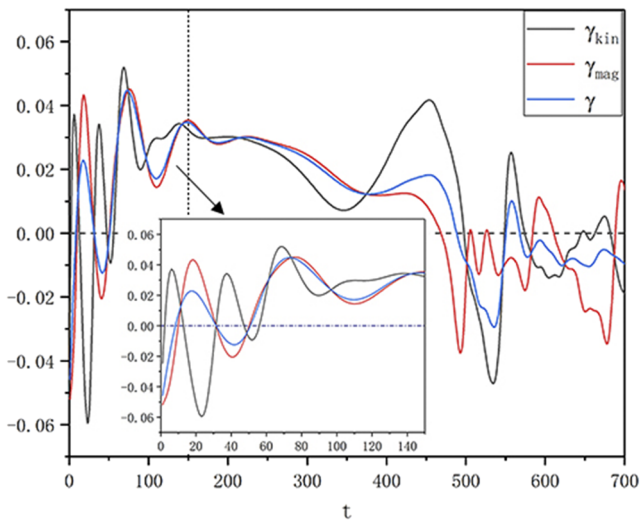


FIG. 8. The evolution of the growth rate of the double tearing mode with $R = 10^8$ and $S = 10^{18}$.

We now study the evolution of the magnetic field line with the change in the growth rate. Figure 8 shows the evolution of the growth rate of the double tearing mode. As can be seen from Fig. 8, at $t = 200$ – 250 (linear development stage), the growth rate is basically constant and the value is about 0.03. At this time, the DTM increases exponentially with a constant growth rate. During the period from $t = 250$ to $t = 350$ (non-linear driving phase), the first batch of magnetic islands grew and the radial positions coincided. Nonlinear coupling occurred between different modes, and the magnetic field line began to enter a period of nonlinear evolution. From $t = 350$ to $t = 450$ (rapid growth phase), the growth rate increases rapidly and the increase in the perturbed kinetic energy is more obvious. This process can be described as follows. The inner and outer magnetic islands exchange radial positions and are connected to the magnetic

field lines, which lead to the disappearance of magnetic islands. At $t = 450$ – 500 (decay phase), the growth rate quickly drops to negative and large-scale magnetic islands disappear. However, after $t = 500$, the amplitude of the perturbation begins to become weak. This corresponds to the process of the generation and disappearance of small magnetic islands.

Since the $m/n = 0/0$ and $3/1$ modes play an important role, we specifically analyze their growth rates here. Figure 9 shows the evolution of the growth rate of $m/n = 0/0$ and $3/1$ modes and the kinetic energy corresponding to the DTM with different modes. In Fig. 9, it is shown that in the whole evolution process, $m/n = 3/1$ perturbed kinetic energy always dominates, but in the process of entering the nonlinear stage, the higher m modes and the $m/n = 0/0$ mode rapidly increase to the magnitude that is similar to the $m/n = 3/1$ mode. The growth rate $\gamma = 0.03$ for $m/n = 3/1$ and $m/n = 0/0$ has no growth in the linear stage. However, the $m/n = 0/0$ mode increases rapidly during the nonlinear stage. We consider several high m modes in the period when the perturbed kinetic energy increases most rapidly around $t = 500$, that is, $m/n = 3/1$, $6/2$, and $9/3$, and the ratio of their peak values of the perturbed kinetic energy is about 5:1.67:1. When finally reaching the saturation stage, the value of the disturbance kinetic energy of $m/n = 3/1$ and $0/0$ tends to be the same value, the $m/n = 6/2$ mode tends to a value, and the rest high m modes tend to another value. The ratio of the three values is about 6:4:1.

In the early stage of magnetic islands ($t = 250$), the plasma is accelerated due to the bending of the magnetic field lines, resulting in a distribution of plasma flow. Figure 10 shows the contour of the poloidal velocity flow of double tearing modes at different times. It is shown that at the O-point of the magnetic island, the poloidal flow velocity of the plasma is relatively small and the poloidal flow velocity around the X-point and O-point edge is large. A vortex is formed on both sides of the two rational surfaces. The two vortices in the middle are coupled into one, and the intensity of the vortex on the outside is greater than that on the inside. At the moment of $t = 440$, the radial positions of the inner and outer magnetic islands coincide and are strongly coupled together. At this time, as the magnetic field

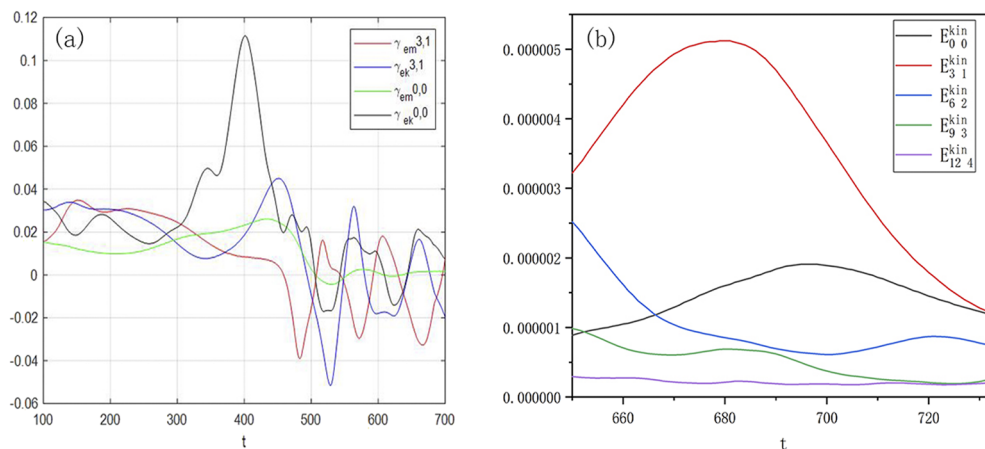


FIG. 9. The evolution of the growth rate (a) and kinetic energy (b) corresponding to the double tearing mode with different modes.

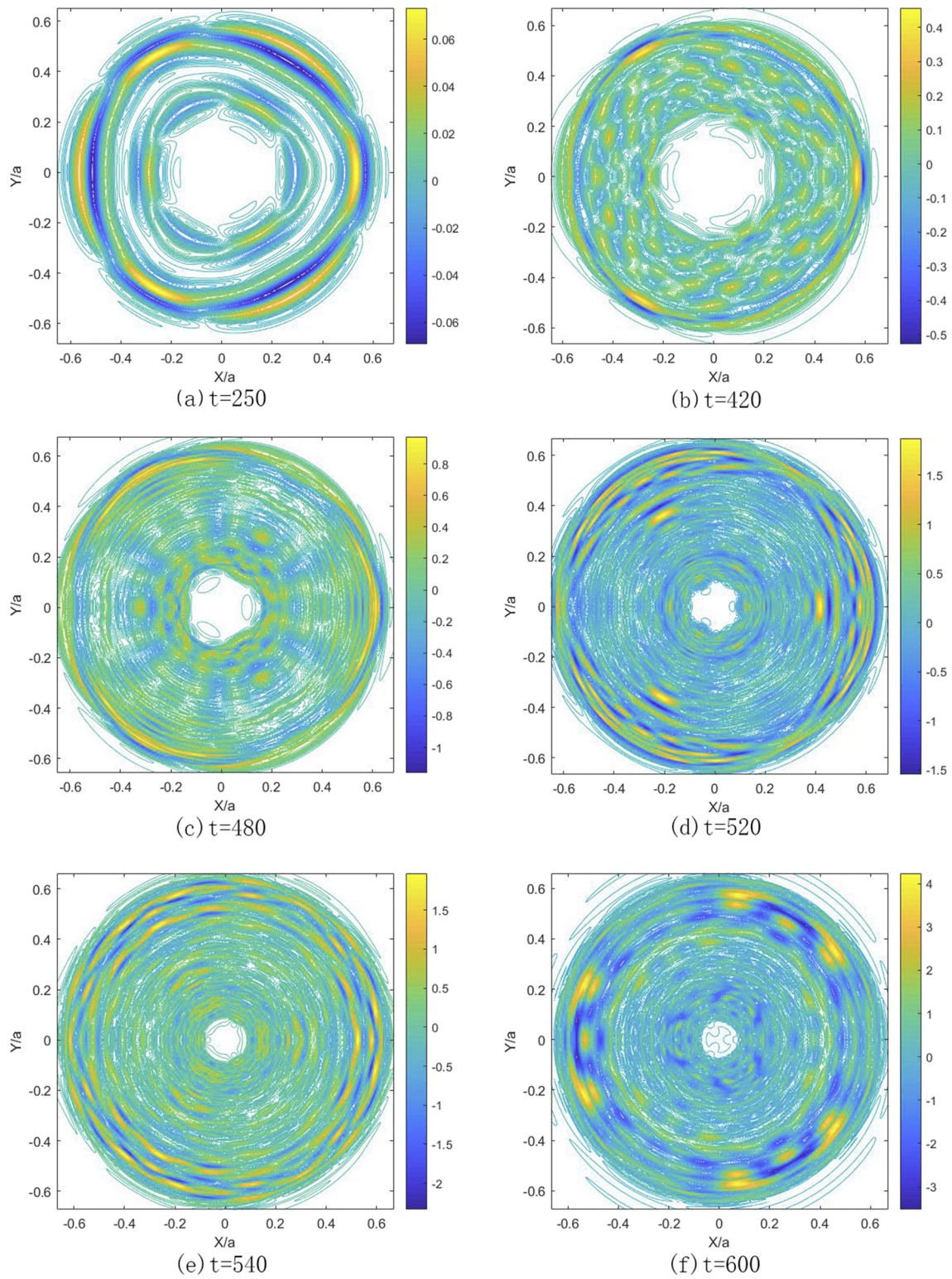


FIG. 10. Contour of poloidal velocity distribution of double tearing modes at different times, $q_s = 3$, $D_{12} = 0.22$, $R = 10^8$, and $S = 10^{18}$: (a) $t = 250$, (b) $t = 420$, (c) $t = 480$, (d) $t = 520$, (e) $t = 540$, and (f) $t = 600$.

lines bend more, the plasma flow field amplitude increases significantly and the distribution range expands. The intensity of shear flow is still large near the rational surface. At $t = 480$, the inner and outer magnetic islands have completed the position exchange and the intensity of the vortex between the two rational surfaces increased.

IV. CONCLUSIONS

The behaviors of nonlinear tearing modes and plasma flows around magnetic islands are studied numerically in a cylindrical geometry, using the method of reduced MHD simulation. It is shown that the single tearing mode reaches a steady state in a relatively short time. The magnetic islands of the double tearing mode on the inner and outer rational surfaces develop to a sufficiently large scale, and their radial positions move and couple with each other when they enter the non-linear phase. It is also shown that the perturbed kinetic energy and magnetic energy of both the single and double tearing modes have a process from oscillation to constant positive values before reaching the linear growth stage.

Concerning the distribution of plasma flow velocity, we find that for the STM island, the shear flow is formed on both sides of the magnetic island and the poloidal flow velocity is larger around the O-point than around the X-point of the magnetic island. There is also a small peak in the poloidal flow velocity at the X-point, while the amplitude of the poloidal flow velocity is weaker at other locations. For the DTM, we found that the peak of the poloidal flow velocity was mainly distributed at the O-point edge and the X-point of the magnetic island, and the plasma flow velocities at the two magnetic island edges are opposite. A vortex is formed on each side of the two rational surfaces. The two vortices in the middle are coupled into one, and the intensity of the vortex on the outside is greater. At the end of the evolution, the inner and outer magnetic islands have completed the position exchange and the intensity of the vortex between the two rational surfaces increased.

A future study may include the implementation of the neoclassical effect in the MHD code, as well as the investigation of kinetic effects of fast ions on the double tearing mode.

ACKNOWLEDGMENTS

This work was supported by the National Key R&D Program of China (Grant Nos. 2018YFE0303102, 2017YFE0301702,

and 2017YFE0301203), NSFC (Grant Nos. 11905109, 11947238, and 11775154), the China Postdoctoral Science Foundation (Grant No. 2018M640230), and U.S. DOE SciDAC ISEP.

DATA AVAILABILITY

The data that support the findings of this study are available from the corresponding author upon reasonable request.

REFERENCES

- ¹Y. Ishii, M. Azumi, G. Kurita, and T. Tuda, *Phys. Plasmas* **7**, 4477 (2000).
- ²Q. Yu and S. Günter, *Nucl. Fusion* **39**, 487 (1999).
- ³J. Li, C. Xiao, Z. Lin, D. Liu, X. Ji, and X. Wang, *Phys. Plasmas* **27**, 042507 (2020).
- ⁴D. Jiaqi, M. Zongze, and L. Yongxing, *Plasma Sci. Technol.* **8**(1), 101 (2006).
- ⁵Z.-X. Wang, L. Wei, and F. Yu, *Nucl. Fusion* **55**, 043005 (2015).
- ⁶Z. X. Wang, X. G. Wang, J. Q. Dong, Y. A. Lei, Y. X. Long, Z. Z. Mou, and W. X. Qu, *Phys. Rev. Lett.* **99**, 185004 (2007).
- ⁷J. Li, X. Ji, J. Dong, Y. Hu, S. Liu, L. Yan, and HL-2A Contributors, *Phys. Plasmas* **26**, 032505 (2019).
- ⁸K. Ida, N. Ohya, T. Morisaki, Y. Nagayama, S. Inagaki, K. Itoh, Y. Liang, K. Narihara, A. Y. Kostrioukov, B. J. Peterson, K. Tanaka, T. Tokuzawa, K. Kawahata, H. Suzuki, and A. Komori, *Phys. Rev. Lett.* **88**(1), 015002 (2002).
- ⁹X.-Q. Wang, X. G. Wang, W.-B. Xu, and Z.-X. Wang, *Phys. Plasmas* **18**, 012102 (2011).
- ¹⁰K. J. Zhao, Y. Nagashima, F. M. Li, Y. Shi, P. H. Diamond, J. Q. Dong, K. Itoh, S.-I. Itoh, G. Zhuang, H. Liu, Z. P. Chen, J. Cheng, L. Nie, Y. H. Ding, Q. M. Hu, Z. Y. Chen, B. Rao, Z. F. Cheng, L. Gao, X. Q. Zhang, Z. J. Yang, N. C. Wang, L. Wang, W. Jin, W. Yan, J. Q. Xu, Y. F. Wu, L. W. Yan, A. Fujisawa, S. Inagaki, Y. Kosuga, M. Sasaki, and J-TEXT Team, *Nucl. Fusion* **57**(12), 126006 (2017).
- ¹¹Z. X. He, J. Q. Dong, Y. X. Long, Z. Z. Mou, Z. Gao, H. D. He, F. Liu, and Y. Shen, *Phys. Plasmas* **17**, 112102 (2010).
- ¹²J. C. Li, C. J. Xiao, Z. H. Lin, and K. J. Wang, *Phys. Plasmas* **24**, 082508 (2017).
- ¹³A. Ishizawa and N. Nakajima, *Phys. Plasmas* **15**, 084504 (2008).
- ¹⁴J. Q. Dong, S. M. Mahajan, and W. Horton, *Phys. Plasmas* **10**, 3151 (2003).
- ¹⁵J. Q. Dong, Y. X. Long, Z. Z. Mou, J. H. Zhang, and J. Q. Li, *Phys. Plasmas* **14**, 114501 (2007).
- ¹⁶J. Q. Dong, Z. Z. Mou, Y. X. Long, and S. M. Mahajan, *Phys. Plasmas* **11**, 5673 (2004).
- ¹⁷Z.-X. Wang, X. Wang, J. Q. Dong, Y. Kishimoto, and J. Q. Li, *Phys. Plasmas* **15**, 082109 (2008).
- ¹⁸T. Voslon, O. Agullo, P. Beyer, M. Yagi, S. Benkadda, X. Garbet, K. Itoh, and S.-I. Itoh, *Phys. Plasmas* **18**, 062302 (2011).
- ¹⁹Q. Hu, Q. Yu, and X. Hu, *Phys. Plasmas* **21**, 122507 (2014).
- ²⁰K. Uzawa, A. Ishizawa, and N. Nakajima, *Phys. Plasmas* **17**, 042508 (2010).